



City Research Online

City, University of London Institutional Repository

Citation: Atkin, C. J. & Gowree, E. R. (2012). Recent Developments to the viscous Garabedian and Korn method. Paper presented at the 28th Congress of the International Council of the Aeronautical Sciences, 23-28 Sep 2012, Brisbane, Australia.

This is the published version of the paper.

This version of the publication may differ from the final published version.

Permanent repository link: <https://openaccess.city.ac.uk/id/eprint/15986/>

Link to published version:

Copyright: City Research Online aims to make research outputs of City, University of London available to a wider audience. Copyright and Moral Rights remain with the author(s) and/or copyright holders. URLs from City Research Online may be freely distributed and linked to.

Reuse: Copies of full items can be used for personal research or study, educational, or not-for-profit purposes without prior permission or charge. Provided that the authors, title and full bibliographic details are credited, a hyperlink and/or URL is given for the original metadata page and the content is not changed in any way.

City Research Online:

<http://openaccess.city.ac.uk/>

publications@city.ac.uk

RECENT DEVELOPMENTS TO THE VISCOUS GARABEDIAN AND KORN METHOD

C J Atkin*, E R Gowree*

***City University London**

chris.atkin.1@city.ac.uk; erwin.gowree.1@city.ac.uk

Keywords: *viscous-inviscid interaction, drag prediction and control*

Abstract

This paper describes recent developments to the legacy VGK method based upon a new coupling with the Callisto boundary layer code developed for Airbus. The new CVGK method has been compared against its predecessor and validated against a transonic swept-wing dataset. Various conceptual studies have then been carried out to model the effect on form drag (viscous pressure drag) of changes to boundary layer entrainment and shock-control ramps. It is concluded that there are both risks to, and opportunities for, drag reduction techniques associated with managing the form drag contribution from the aft region of highly-loaded transonic aerofoils.

1 Introduction

This paper describes recent developments to the legacy VGK method (viscous Garabedian & Korn [1]) first developed at the Royal Aircraft Establishment in the late 1970s [2] and used extensively to explore supercritical wing design philosophy for the next twenty five years or so. The method employs viscous-inviscid analysis (VII): the conformal-mapping, full-potential method of G&K is used to calculate the inviscid flow, with modifications to allow the accurate prediction of shock waves up to shock Mach numbers of 1.3 or so; the viscous effects are calculated using the Lag-Entrainment integral method for turbulent boundary layers developed by Green et al [3] and refined in the 1980s by Ashill et al [4], first as Advanced VGK (AVGK) and later as ‘B’VGK.

The Lag-Entrainment method has proved to be very capable of capturing the history effects in turbulent boundary layer flows,

standing comparison with some of the more sophisticated turbulence models used in Reynolds-Averaged Navier Stokes (RANS) methods.

VII methods are of course limited in their ability to capture large-scale flow separation. Nevertheless, attached flow represents the norm for many design points and VII methods remain extremely rapid alternatives to RANS methods for optimisation applications and aeroelastic analysis where fast turnaround is required. As pointed out by Lock & Williams [5] the VII approach also facilitates the accurate breakdown of aerodynamic drag into the vortex, wave, friction and form (viscous pressure) drag components. Full-potential methods such as G&K also give far more accurate predictions of the development of the flow at the stagnation point of an aerofoil (the attachment line in 3D) than current RANS methods based upon finite-volume Euler schemes. Accurate knowledge of the flow gradients in the vicinity of the attachment line of a swept wing is essential for establishing the correct development of laminar crossflow instability in the study of Laminar Flow Control (both Natural and Hybrid).

2 Numerical approach

The current incarnation of VGK is based upon a new coupling of the modified G&K solver with the Callisto boundary layer code developed by the first author for Airbus over the last decade.

Callisto is an implementation of Ashill & Smith’s [6] version of Smith’s earlier three-dimensional integral boundary layer method, simplified for swept and tapered wings, but also incorporating the higher-order boundary layer effects which were later added to BVGK [4].

The geometric assumptions are illustrated in Figures 1 and 2 below: the wing is locally assumed to be of constant section and twist, and the leading and trailing edges meet at a point O . In fact any radius r joining the origin O with a point on the wing surface should lie along a generator of the wing.

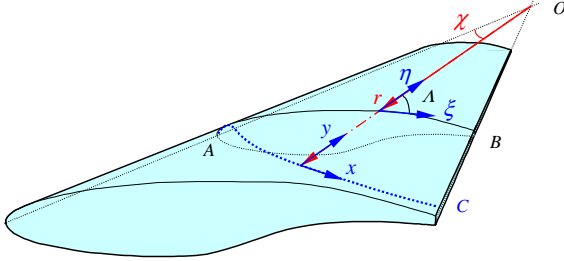


Fig. 1. Schematic of a swept-tapered wing.

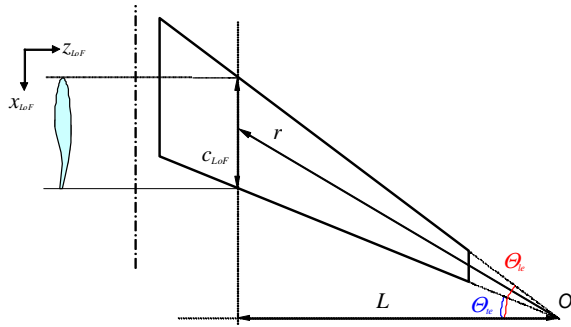


Fig. 2. Plan view of a swept-tapered wing.

The swept-tapered symmetry extends to the external inviscid flowfield such that isobars of surface pressure also lie along the wing generators, and also to most of the viscous flow properties which are also assumed to be invariant along the span of the wing. The exception is the boundary layer length scale which is taken as proportional to local line-of-flight chord length for turbulent flows, and to the square root of local chord for laminar flows.

The principal governing equation is the well-known momentum integral equation of von Karman with added higher order terms (HOT) to capture the effects of viscous flow curvature and Reynolds normal stresses:

$$\frac{d\theta}{dx} = \frac{c_f}{2} - (2 - M_c^2 + H) \frac{\theta}{u_e} \frac{du_e}{dx} + HOT \quad (1)$$

The unknown shape factor H is the subject of a further governing equation for the entrainment

of the neighbouring inviscid flow by the growing boundary layer:

$$H_1 \frac{d\theta}{dx} + \frac{dH_1}{dH} \frac{dH}{dx} = c_E - H_1 \frac{\theta}{u_e} \frac{du_e}{dx} \quad (2)$$

Equation (2) includes two further unknowns, H_1 and c_E . The former is found to be a function only of H , and can therefore be calculated, while the latter is the *entrainment coefficient* which is determined by the intensity and structure of the turbulence in the viscous layer. This then introduces a third governing equation, the Lag equation of Green et al [3] which is effectively a model of turbulence. The von Karman equation (1) can be applied to three-dimensional flows by adopting the streamline analogy which assumes that the equation can be applied to the flow properties as resolved along the inviscid streamline immediately adjacent to the viscous flow. Higher-order methods (including Callisto) further refine the concept to consider the surface streamline of the equivalent inviscid flow (defined as the purely inviscid flow which shares the same streamline patterns as the inviscid part of the real viscous flow) but this is more than enough detail for the present paper. Equations (1) and (2), along with the spanwise variation of the momentum thickness θ derived from the swept-tapered assumptions already mentioned, provide a system of equations for the variation of θ and H in both x and y directions (Fig. 1), although Callisto actually solves the equations in the non-orthogonal (ξ, η) co-ordinate system (also shown in Fig. 1).

The method can be used as a stand-alone analysis tool for experimental pressure distributions, or coupled to an inviscid computational method, in which case the displacement effect of the boundary layer is fed back to the inviscid solver as a transpiration boundary condition. As with most such methods, the viscous equations can be solved in inverse mode to get beyond the singular case of separation, necessitating a slight change to the coupling technique to the inviscid solver [5]. However this approach is limited to mild separation for which the basic premise of thin viscous layers still holds. Notwithstanding this limitation, a properly coupled VII method has some attractive features in terms of modelling

the flow at the trailing edge of a wing, seemingly a challenge for Navier-Stokes methods which often produce a large spike in pressure at a sharp trailing edge. The B/CVGK methods actively enforce the Kutta condition by ensuring, by adjustment of the transpiration boundary conditions supplied to the inviscid solver, that the pressures on either side of the trailing edge are both finite and equal.

The swept-tapered approximation can be applied both to quasi-two-dimensional flows for which the pressure distribution is truly invariant along the span and to simple three-dimensional flows where the variation of geometry and chord-wise pressure distribution is slight, so that the three-dimensional flow can be treated as a series of locally swept-tapered problems with slightly different boundary conditions. Although this is an unnecessary simplification given the available computational power today, it is nonetheless a valuable simplification if speed is of the essence, for example if repeatedly calculating transition fronts or if coupling with some kind of optimiser.

The rationale behind the Callisto development was to develop a Lag-Entrainment code which could be coupled to many different inviscid solvers, and indeed to allow the coupling framework to be exploited by other boundary layer methods. This has pretty much been achieved, Callisto having been coupled to the BAE Systems Flite3D unstructured Euler method, to Fluent and to the G&K method. Work is also currently under way to couple Callisto to the DLR TAU method. Callisto is coded as a shared library accessed by the inviscid solvers and therefore the same modelling, implemented via the same lines of code, features in each implementation. This allows the transfer of flow control modelling between the methods with some confidence. Recent developments to Callisto, to allow the modelling of flow control devices such as sub-boundary layer vortex generators, surface suction panels for laminar flow control as well as excrescence drag modelling by the manipulation of boundary layer integral parameters, are therefore available to all these methods. This re-use of modelling is believed to have no parallels among Navier-Stokes solvers.

For the particular case of high aspect-ratio wings it can be valuable to investigate flow control concepts within the swept-tapered, quasi-two-dimensional approximation before applying to more realistic wing-body configurations. In order for the two-dimensional VGK method to exploit the swept-tapered modelling of the boundary layer by Callisto, pre- and post-processing has been added to the inviscid G&K method to implement Lock's transformations [7] for infinite-swept and swept-tapered wings to extend the capabilities of the rapid aerofoil analysis to swept-tapered flows.

In the past the co-ordinate systems for VII analysis of swept-tapered wings have precluded the analysis of the wake flow more than a certain distance downstream of the wing trailing edge but this difficulty has been overcome in Callisto so that the wake development can be calculated right through to the Trefftz plane (downstream infinity), allowing the viscous drag to be computed without recourse to the formula of Squire and Young [8] and its derivatives (e.g. Cooke [9]).

3 Objectives

Reporting of these capabilities and the design trends which they elicit will require a number of articles. The current paper will focus upon the validation of the drag predicted by the Callisto-VGK method (CVGK) and the exploration of form drag control, a topic which has received little attention in the literature.

4 Validation of CVGK against experiment

The experimental data chosen for validation of the CVGK drag predictions (viscous and wave drag) are taken from the report of Ashill et al [10] who studied the flow over aerofoil models swept back at 25° in the RAE 8ft tunnel at high-subsonic speeds. The models tested during this campaign were un-cambered derivatives of the RAE 52XX family designed to replicate a variety of trailing edge pressure recovery strategies without the complications associated with wind-tunnel lift corrections or the

interference of trailing vorticity (the models were tested at zero incidence).

The tests covered a Mach number range between 0.6 and 0.85 at two unit Reynolds numbers of 14.4 and 31.2 per metre (wing chord was 475mm). Centre and tip bodies were used to ensure that the flow was invariant along most of the span of the model and both surface pressures and wake pitot pressures were obtained, as well as overall force measurements. Transition was fixed using an air injection method to minimise excrescence drag due to tripping. The data obtained thus offer an excellent basis for validating simple swept-wing methods such as CVGK, capturing as they do both sweep and transonic effects up to and including boundary layer separation.

Figures 3 and 4 below show the experimental data for two cases, RAE 5237 and RAE 5240, including error estimates [10], plotted with the drag predicted by both CVGK and BVGK. The results are excellent, lying within or just outside the bound of experimental error, with a difference between computation and experiment of the order of two drag counts.

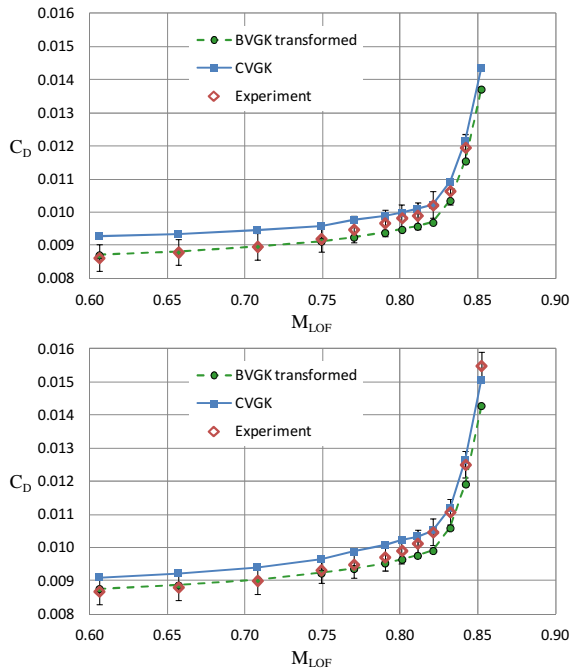


Fig. 3. Zero-lift drag development for 25°-swept RAE 5237 (top) and 5240 (bottom) sections, at increasing Mach number, unit Reynolds number 14.4 million per metre. Experimental data, 2D BVGK analysis with sweep transformations, and 3D (infinite-swept) CVGK analysis.

For both VGK methods the total drag is compiled by combining overall viscous drag with post-processed wave drag from the inviscid flowfield, using the MACHCONT process developed by the Aircraft Research Association.

For CVGK, the viscous drag is obtained from the far-field momentum thickness determined by Callisto so that the extracted drag is aggregated as follows:

$$C_{D,3D} = C_{D_v,3D} + C_{D_w,2D} \times \cos^3 \Theta \quad (3)$$

where C_{D_v} is viscous drag and C_{D_w} is wave drag, Θ being the sweep angle illustrated in Figure 2 (in this case for an untapered planform). For BVGK, the two-dimensional viscous drag is subdivided and scaled as follows:

$$C_{D,3D} = C_{D_f,2D} \times \cos^{0.2} \Theta + C_{D_p,2D} \times \cos^3 \Theta \quad (4)$$

where C_{D_f} is friction drag coefficient and C_{D_p} is pressure drag coefficient, comprising both wave drag and form drag in the present case. Here the friction drag is scaled using simple Reynolds number trends for 2D turbulent flow [10].

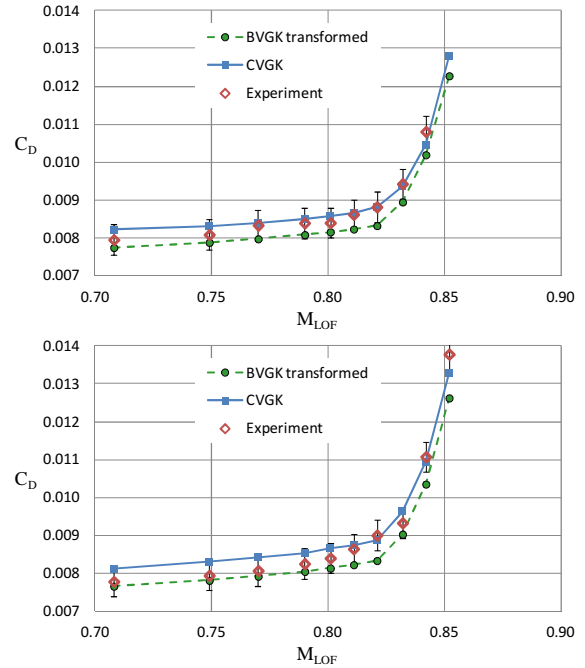


Fig. 4. Zero-lift drag development for 25°-swept RAE 5237 (top) and 5240 (bottom) sections, at increasing Mach number, unit Reynolds number 31.2 million per metre. Experimental data, 2D BVGK analysis with sweep transformations, and 3D (infinite-swept) CVGK analysis.

Ashill et al [10] also present the results of their own analysis using both BVGK and their own version of VGK with sweep effects, SWVGK, which method appears not to have been widely disseminated. Their BVGK results look very similar to those presented here (relative to the experimental results) but the SWVGK results in [10] lie below the BVGK results, unlike the CVGK trends shown above.

Figure 5 below illustrates that the surface pressure distributions are also well captured by the VII methods, even with quite strong shock waves, although at Mach 0.84 it is clear that the methods underestimate the strength of the shock wave. This is also clear from the drag results for this case, presented in Figure 4.

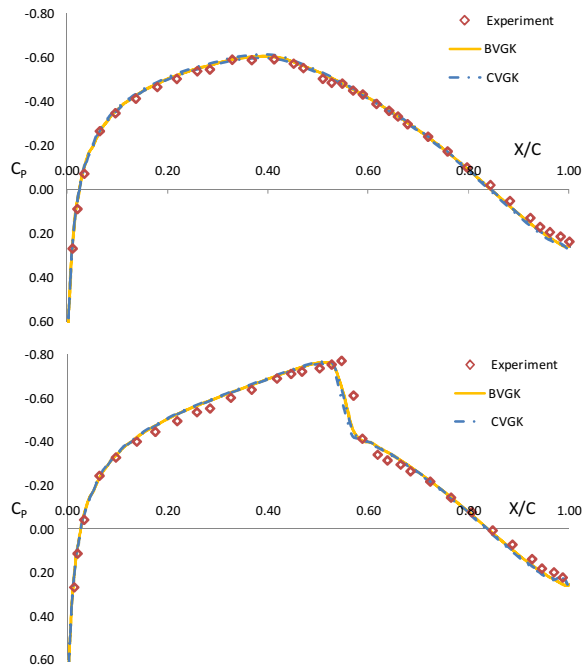


Fig. 5. Zero-lift pressure distributions for 25°-swept RAE 5240 section, at Mach 0.81 (top) and 0.84 (bottom), unit Reynolds number 31.2 million per metre. Experimental data, 2D BVGK analysis with sweep transformations, and 3D (infinite-swept) CVGK analysis.

The swept-tapered boundary layer analysis in Callisto suggests that the assumptions present in equation (4) are not entirely confirmed in practice. Figure 6 illustrates the differences in friction and form drag obtained from BVGK and CVGK, for both 2D and swept cases, where the swept results have been converted back to an ‘equivalent’ two-dimensional value using equation (4) above. Figure 6 shows that,

according to Callisto, sweep has a greater than assumed influence on both drag components, reducing the relative contribution of friction drag and increasing the relative contribution of form drag. The net effect here is an increase in overall viscous drag, which explains why the CVGK drag values are slightly higher than the transformed BVGK values in Figures 3 and 4 above; the two methods give almost identical results for two dimensional aerofoil analyses.

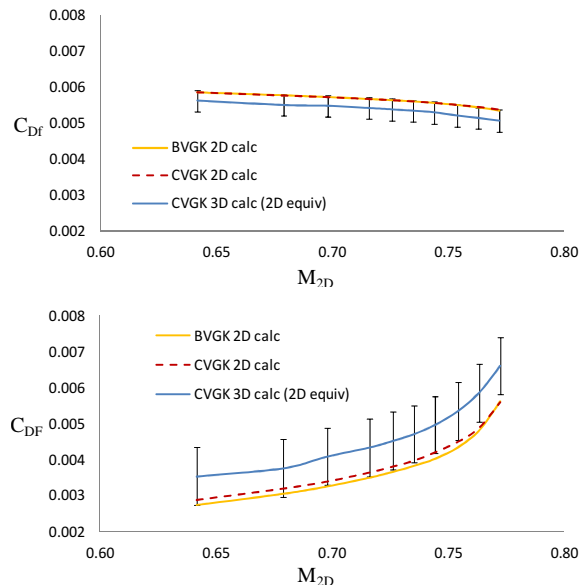


Fig. 6. Equivalent two-dimensional friction (top) and form (bottom) drag coefficients for 25°-swept RAE 5240 section, at increasing Mach number, unit Reynolds number 31.2 million per metre.

The BVGK method has not been actively developed for some time and is hard-coded with a ‘recommended mesh size of 160 points around the aerofoil and 32 points from aerofoil to far-field boundary. The development of CVGK allowed the implementation of a reliable mesh refinement capability, the results of which are illustrated in Figure 7. BVGK does allow a preliminary analysis on a coarser mesh, so mesh sizes of 80 x 16, then 160 x 32 would be used to obtain a solution. For CVGK the mesh sequence was 60 x 12, then 120 x 24, then 240 x 48. Convergence characteristics for one of the RAE 5240 test cases are shown in Figure 8.

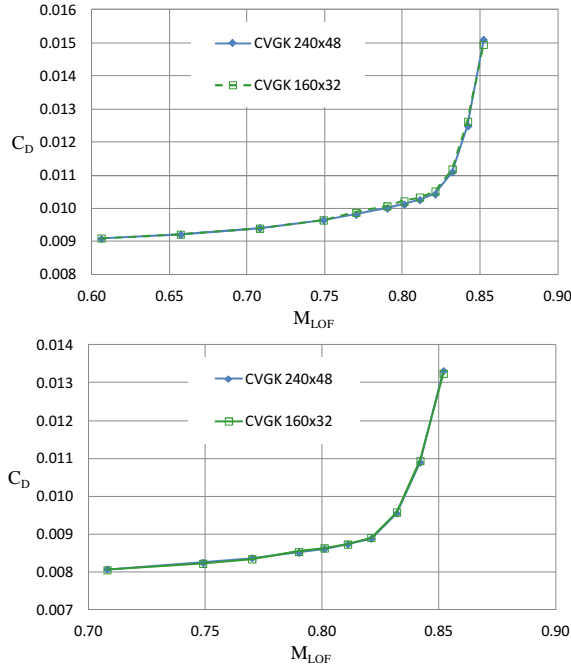


Fig 7. Zero-lift drag development for 25°-swept RAE 5240 sections, at increasing Mach number, unit Reynolds number 14.4 (top) and 31.2 (bottom) million per metre. Comparison of 160 x 32 and 240 x 48 meshes.

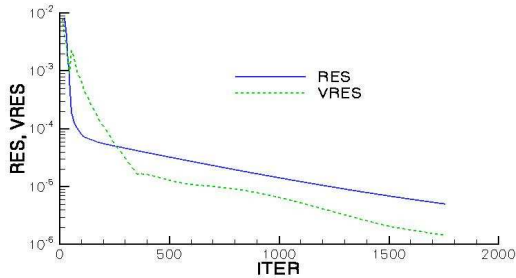


Fig. 8. CVGK convergence for 25°-swept RAE 5240 section, at Mach 0.8, unit Reynolds number 14.4 million per metre. 240 x 48 mesh.

The preceding results provide a platform to demonstrate both the advantages of low-order methods such as Callisto and a new ‘inverse design’ approach to flow control: namely, instead of investigating the properties of a given flow-control device, rather identify flow mechanisms which could be excited to deliver a performance benefit – by some, as yet unidentified, flow actuation scheme.

5 Form Drag – the Ugly Sister

Current drag reduction research focusses almost exclusively on the reduction of skin friction drag. However, particularly for lifting surfaces, the contribution from form drag is more

significant and warrants at least some attention, even though skin friction schemes will reduce both components of profile drag.

5.1 Origin of Form Drag

Form drag is best explained using a preliminary form of the von Karman equation (1) which is reached before the boundary layer edge density ρ_e and velocity u_e terms are eliminated:

$$\frac{d}{dx}(\rho_e u_e^2 \theta) = \tau_{wall} - \delta^* \frac{dp}{dx} \quad (5)$$

where τ_{wall} is the wall shear stress, δ^* is the displacement thickness and p is the local static pressure. Equation (5) can be integrated with respect to streamwise distance x to yield:

$$\rho_\infty u_\infty^2 \theta_\infty = \int_0^\infty \tau_{wall} dx + \int_{x=0}^{x=\infty} \delta^* dp \quad (6)$$

The left-hand side should be familiar to the reader as total viscous drag per unit span since, for an aerofoil section,

$$C_D = 2 \frac{\theta_\infty}{c} \quad (7)$$

The right-hand side of equation (6) consists of the integrated friction and one further term equal to the product of the displacement thickness and the pressure change experienced by the boundary layer. This is the form drag term, familiar to those designing low-Reynolds-number aerofoils because of the dominating effect of separation bubbles and their major impact upon drag. It is instructive to look at the development of form drag on a lifting transonic aerofoil. Here the example considered is the RAE 2822 aerofoil. The pressure distribution is shown in Figure 9 below and the chord-wise evolution of drag components in Figure 10.

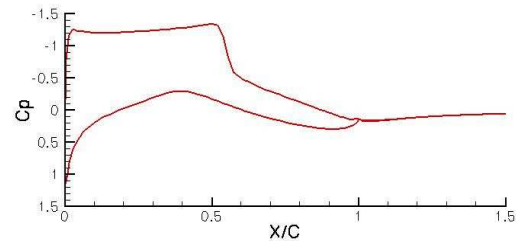


Fig. 9. Pressure distribution for un-swept RAE 2822 aerofoil, at Mach 0.73, Reynolds number 6.5 million, incidence 3.2°: ‘Case 9’ of AGARD AR 138 [11].

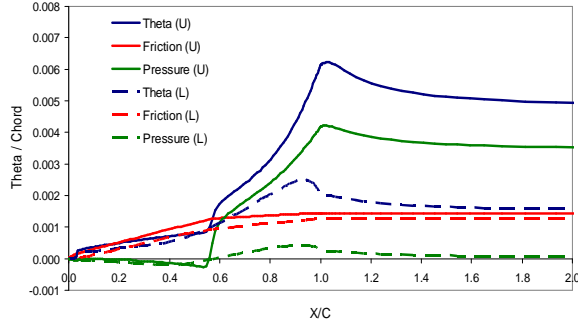


Fig. 10. Development of friction, form (pressure) and profile (θ) drag components on the upper (solid) and lower (dashed) surfaces of the RAE 2822 aerofoil shown in Figure 9.

Figure 10 illustrates how the friction drag term develops principally over the front half of the aerofoil chord, remaining fairly static over the rear part of the aerofoil. Conversely the form (pressure) drag development is negligible until the start of the adverse pressure gradient over the rear part of the aerofoil. In fact – on the upper surface – the shock and aft pressure recovery regions contribute twice as much drag (through form drag) than the forward, friction-dominated region.

Clearly the form drag depends upon the early development of the boundary layer displacement thickness through the action of friction, but friction plays no further part in the development of this drag component over the rear end of the aerofoil. So, although it is well understood that the reduction of skin friction, either by laminar flow control or by control of near-wall turbulent structures, will lead to an overall reduction in profile drag (both friction and form components), it is perhaps less well publicised that there are opportunities to manage form drag itself over the critical region of adverse pressure gradient.

5.2 Control of Form Drag

For a given lift requirement (which normally determines the magnitude of the pressure gradients over the aerofoil), form drag can be controlled by management of the displacement thickness, defined by the product of momentum thickness and shape factor:

$$\delta^* = H\theta \tag{8}$$

Equation (8), along with equation (2), offers the opportunity to manage the growth in displacement thickness by *increasing the entrainment* in the boundary layer (since dH_1/dH is negative for attached boundary layers). Entrainment of energetic fluid is precisely the function of most separation control devices, such as vortex generators. The effect of enhanced entrainment can be modelled by increasing (artificially, at present) the magnitude of the entrainment coefficient in equation (2) above.

Four scenarios have been considered. In the first, the effect of 10% greater entrainment over the entire upper surface of the aerofoil has been modelled. In the second scenario, a 20% increase in entrainment has been modelled across the upper surface. In the third scenario, this 20% increment has been applied to the upper surface but only aft of the mid-chord position. In the final scenario, the entrainment aft of mid-chord has been increased by 50%. The results are shown in Table 1 below, and the effect on the displacement thickness and shape factor of control strategy 4 is shown in Figure 11 below.

Case	C_D
Baseline	0.0127
Control 1: $\Delta c_E = +10\%$ throughout	0.0125
Control 2: $\Delta c_E = +20\%$ throughout	0.0126
Control 3: $\Delta c_E = +20\%$ aft of shock	0.0125
Control 4: $\Delta c_E = +50\%$ aft of shock	0.0119

Table 1. Effects of augmenting entrainment over the upper surface of the RAE 2822 aerofoil under the flow conditions shown in Figure 9.

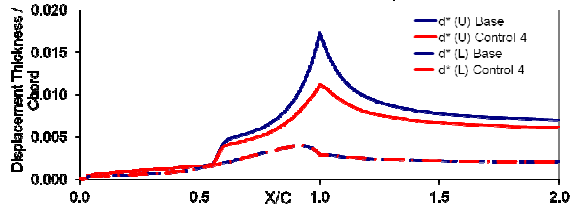


Fig. 11. Development of displacement thickness on the upper (solid) and lower (dashed) surfaces of the RAE 2822 aerofoil under the flow conditions shown in Figure 9, with entrainment control scenario 4 (Table 1 above).

At this stage nothing has been said about the kind of device which might deliver this kind of action. Green et al [3] define the relationship between the entrainment and skin friction

coefficients and the peak Reynolds shear stress (for incompressible flow) as follows:

$$\frac{\tau_{Reynolds,max}}{\rho_e u_e^2} = 0.024c_E + 1.2c_E^2 + 0.32c_f \quad (9)$$

This relationship suggests a close correlation between entrainment and Reynolds shear stress, so any device which could increase the turbulence intensity in the adverse pressure gradient region of an aerofoil should have a beneficial effect on drag as well as the more conventional goal of delaying the onset of flow separation in the presence of strongly adverse pressure gradients.

Clearly any such flow control device might incur an excrescence drag penalty which has not been modelled here. However the primary purpose of this work has been to demonstrate the possibility of independent control of the form drag component which, for highly loaded aerodynamic surfaces, makes up about two thirds of the overall viscous drag budget. In particular, entrainment is driven by integral length scales which scale with boundary layer thickness, while skin friction control is concerned with the much smaller structures near the wall. Entrainment control may therefore be easier to implement at high Reynolds number.

The secondary purpose of this study has been to demonstrate that the simpler equations used in the boundary layer approach can provide some insight into flow control opportunities which is less easily obtained from the analysis of the results from field methods such as Navier Stokes solvers.

5.3 Shock control

The boundary layer equations can similarly be used to carry out some conceptual studies on shock control. The basic idea behind shock control is to develop the single, normal shock into a lambda structure involving two oblique shocks, thus reducing the total pressure loss across shock. In order to achieve this, the leading edge of the lambda must be induced by a deflection of the streamlines just outside the boundary layer, and this deflection must be mirrored in the displacement surface of the

boundary layer. This can be simulated by augmenting the value of δ^* in the boundary layer calculation, which can easily be done by introducing a step in H . The test case for this exercise is RAE 2822 again, but this time at 2.5° incidence ('case 7' from [11]). This case has a weaker shock than case 9, but still at about 50% chord. Four control scenarios are considered:

- introducing a 10% increase in δ^* (alone) at 25% chord;
- introducing a 10% increase in δ^* (alone) at 48% chord;
- introducing 10% increases in both δ^* and θ at 25% chord; and
- introducing 10% increases in both δ^* and θ at 48% chord.

The impact of control scenarios 1 and 3 are difficult to discern in the plots of the results, but scenarios 2 and 4 are shown below in Figure 12.

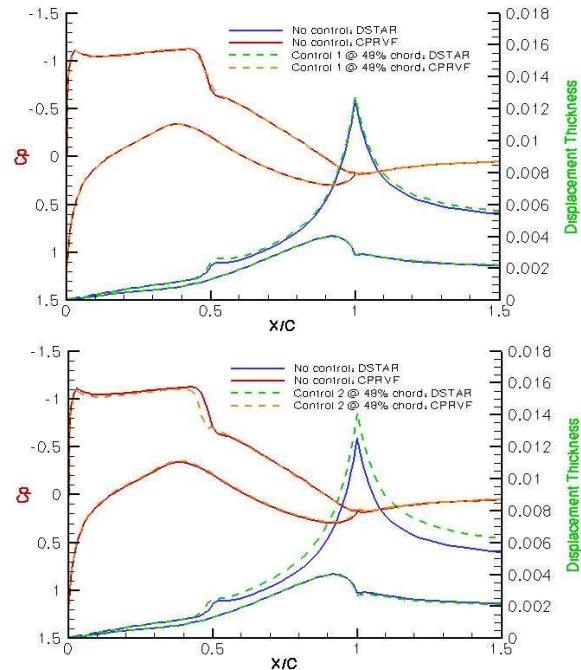


Fig. 12. Surface pressure and displacement thickness distributions on the RAE 2822 aerofoil at Mach 0.725, Reynolds number 6.5 million, incidence 2.5° with and without a viscous ramp at 48% chord. In the upper figure the control is applied only to displacement thickness δ^* ; in the lower figure, to both δ^* and θ .

For both of the examples shown in Figure 12, there is both a smearing of the shock pressure rise – indicative of the formation of a lambda shock – and an increase in the

displacement thickness just ahead of the pressure recovery over the rear part of the aerofoil upper surface. In both cases there is a reduction in wave drag but a *greater* increase in form drag, which is more marked when the momentum thickness is also subjected to an increment, as might be expected. This increase in form drag is associated both with the pressure recovery aft of the shock and with the shock jump itself. Shock drag control techniques should therefore be evaluated in the presence of realistic downstream pressure distributions, rather than under idealised conditions.

Interestingly, of the two control scenarios involving input at 25% chord, one (δ^* alone) actually achieves a small drag reduction. This is because the viscous ramp is introduced ahead of a region of favourable pressure gradient. This benefit disappears when the momentum thickness is also subjected to an increment, for example if there were to be some excrescence drag associated with the viscous ramp.

6 Conclusions

The latest incarnation of the Viscous Garabedian and Korn aerofoil method, CVGK, has been validated against drag measurements on non-lifting, transonic swept wings. A mesh refinement study has also been carried out. Both activities have given confidence in the method for studying flow control schemes for drag reduction.

The formulation of the governing equations allows for intervention in the development of entrainment coefficient, and directly in the distributions of displacement and momentum thickness, without the need for an established concept for a flow control device. While such studies are rather abstract, then can inform the community about research areas which might be prove profitable or otherwise.

Acknowledgements

The authors would like to acknowledge the financial contribution of EADS Innovation Works (UK), which supported part of the work, and the permission granted by Airbus UK to use Callisto for these studies.

References

- [1] Garabedian P R and Korn D G. Analysis of transonic airfoils. *Communications on Pure and Applied Mathematics*, Vol. 24, issue 6, 1971.
- [2] Collyer M R and Lock R C. Prediction of viscous effects in steady transonic flow past an aerofoil. *Aeronautical Quarterly*, Vol. 30, 1979.
- [3] Green J E, Weeks D J and Brooman J W F. Prediction of turbulent boundary layers and wakes in compressible flow by a lag-entrainment method. *ARC R&M 3791*, 1973.
- [4] Ashill P R, Wood R F and Weeks D J. An improved, semi-inverse method of the viscous Garabedian and Korn method (VGK). *RAE Technical Report 87002*, 1987.
- [5] Lock R C and Williams B R. Viscous-inviscid interactions in external aerodynamics. *Prog. Aerosp. Sci.* Vol. 24, 1987.
- [6] Ashill P R and Smith P D. An integral method for calculating the effects on turbulent boundary layer development of sweep and taper. *Aeronautical Journal*, February 1985.
- [7] Lock R C. An equivalence law relating three- and two-dimensional pressure distributions. *NPL Aero Report no. 1028*, July 1962.
- [8] Squire H B and Young A D. The calculation of the profile drag of aerofoils. *ARC R&M 1838*, 1937.
- [9] Cooke J C. The drag of infinite swept wings with an addendum. *ARC CP 1040*, 1969.
- [10] Ashill P R, Fulker J L and Wood R F. On the sectional drag and pressure distributions of swept-wing aerofoil sections. *RAE Technical Report 88073*, 1988.
- [11] Cook P H, McDonald M A and Firmin M C P. Aerofoil RAE 2822 – pressure distributions and boundary layer and wake measurements. *AGARD-AR-138*, section A6, 1979.

Copyright Statement

The authors confirm that they, and/or their company or organization, hold copyright on all of the original material included in this paper. The authors also confirm that they have obtained permission, from the copyright holder of any third party material included in this paper, to publish it as part of their paper. The authors confirm that they give permission, or have obtained permission from the copyright holder of this paper, for the publication and distribution of this paper as part of the ICAS2012 proceedings or as individual off-prints from the proceedings.